

Semi-Supervised End-To-End Contrastive Learning For Time Series Classification

Huili Cai*
Hohai University
huilicai0721@hhu.edu.cn

Xiang Zhang*
University of North Carolina at Charlotte
xiang.zhang@charlotte.edu

Xiaofeng Liu
Hohai University
xfliu@hhu.edu.cn

Abstract

Time series classification is a critical task in various domains, such as finance, healthcare, and sensor data analysis. Unsupervised contrastive learning has garnered significant interest in learning effective representations from time series data with limited labels. The prevalent approach in existing contrastive learning methods consists of two separate stages: pre-training the encoder on unlabeled datasets and fine-tuning the well-trained model on a small-scale labeled dataset. However, such two-stage approaches suffer from several shortcomings, such as the inability of unsupervised pre-training contrastive loss to directly affect downstream fine-tuning classifiers, and the lack of exploiting the classification loss which is guided by valuable ground truth. In this paper, we propose an end-to-end model called SLOTS (Semi-supervised Learning fOr Time clasSification). SLOTS receives semi-labeled datasets, comprising a large number of unlabeled samples and a small proportion of labeled samples, and maps them to an embedding space through an encoder. We calculate not only the unsupervised contrastive loss but also measure the supervised contrastive loss on the samples with ground truth. The learned embeddings are fed into a classifier, and the classification loss is calculated using the available true labels. The unsupervised, supervised contrastive losses and classification loss are jointly used to optimize the encoder and classifier. We evaluate SLOTS by comparing it with ten state-of-the-art methods across five datasets. The results demonstrate that SLOTS is a simple yet effective framework. When compared to the two-stage framework, our end-to-end SLOTS utilizes the same input data, consumes a similar computational cost, but delivers significantly improved performance. We release code and datasets at <https://anonymous.4open.science/r/SLOTS-242E>.

1 Introduction

Time series data, a sequence of data points collected at regular intervals over time [1], is prevalent across various fields such as economics, meteorology, healthcare, and transportation [2,3,4,5,6,7]. However, time series analysis often faces limitations of the scarcity of data labels. Factors such as domain expertise requirements, extensive manual efforts, and privacy concerns constrain the acquisition of high-quality data annotations [8]. Unsupervised (or self-supervised) contrastive

*co-first author.

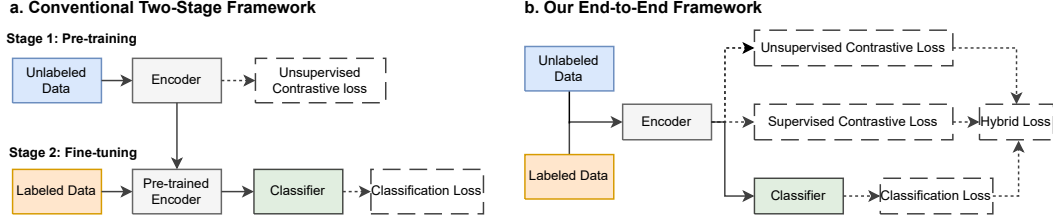


Figure 1: (a) Illustration of a standard self-supervised contrastive model for classification tasks. The whole framework includes two stages: pre-training and fine-tuning. (b) Proposed end-to-end framework. Our model exhibits two properties that are unattainable in conventional two-stage frameworks: 1) the unsupervised contrastive loss, calculated on unlabeled data, contributes to the optimization of the classifier, enabling more effective utilization of the unlabeled data; 2) the incorporation of a newly added supervised contrastive loss further enhances performance and facilitates more efficient learning, resulting in a more powerful and robust model.

learning has emerged as a significant and effective technique for learning valuable representations from time series data without relying on labels [9]. This approach operates by prompting the model to generate similar representations for distinct views or augmentations of the same data instance, while simultaneously driving the representations of different instances further apart [10,11,12].

The majority of existing unsupervised contrastive learning methods follow a two-stage paradigm [13,14], as illustrated in Figure 1 (a). First, during the pre-training stage, an unlabeled dataset is fed into an encoder that maps the input data sample to a latent space. In this space, a contrastive loss is calculated based on instance discrimination. The unsupervised contrastive loss is then used to optimize the encoder [15,16,17]. Subsequently, in the fine-tuning stage, a small-scale labeled dataset is fed into the pre-trained model to generate representations. A supervised classification loss is calculated to optimize the classifier and/or fine-tune the encoder.

While the two-stage contrastive learning approach has demonstrated effectiveness in various domains, it also presents challenges that may hinder better performance. One notable shortcoming of this process is that the unsupervised pre-training contrastive loss cannot directly influence downstream fine-tuning classifiers, potentially limiting the optimization of the final model. Furthermore, this approach fails to fully exploit the classification loss, which is guided by valuable ground truth information. As a result, the potential benefits of incorporating such information during the learning process are not fully realized in the traditional two-stage contrastive learning framework. Moreover, considering the two stages as a whole, it becomes evident that the self-supervised learning framework actually receives a semi-supervised dataset (integrating unlabeled samples in pretraining and labeled samples in fine-tuning). Then, a natural idea is to directly design a semi-supervised end-to-end model to fully exploit the semi-labeled data.

To address these questions, we propose an end-to-end contrastive framework named SLOTS (Semi-supervised Learning fOr Time clasSification), as shown in Fig. 1 (b). The end-to-end model allows for the simultaneous training of the encoder and classifier, unifying model optimization, reducing intermediate computational resources, and learning task-specific features. SLOTS takes a semi-labeled dataset as input, which is identical to that of a conventional two-stage framework. Compared to a traditional two-stage framework, our SLOTS: 1) receives the same dataset (partially unlabeled and partially labeled samples); 2) has the same model components (an encoder and a classifier); and 3) calculates not only the unsupervised contrastive loss and supervised classification loss but also introduces a supervised contrastive loss, computed with available true labels (see ablation study).

Regarding loss functions, unsupervised contrastive loss learns representations by maximizing agreement between differently augmented views of the same unlabeled sample. Supervised contrastive learning brings samples with same categories closer to each other using a supervised contrastive loss in the embedding space. To jointly train the end-to-end framework, we develop a hybrid loss that weighted aggregates unsupervised contrastive loss, supervised contrastive loss, and classification loss.

We note the trade-off between adaptability and model performance. While two-stage models may be more effective in transfer learning or situations where pre-training and fine-tuning involve different datasets, our SLOTS model is a superior choice for achieving optimal performance on a specific dataset (Section 5; Appendix E). We evaluate the SLOTS model on five time series datasets covering a large set of variations: different numbers of subjects (from 15 to 38,803), different scenarios

(neurological healthcare, human activity recognition, physical status monitoring, etc.), and diverse types of signals (EEG, acceleration, and vibration, etc.). We compare SLOTS to ten state-of-the-art baselines. Results show that SLOTS outperforms the two-stage baselines with an improvement of up to 16.10% in the F1 score with only 10% labeled data on the emotion recognition dataset DEAP [18]. Furthermore, SLOTS achieves the highest performance with substantial margins (3.55% on average in F1 score) compared with the strongest baselines on broad tasks.

2 Related Work

Self-supervised contrastive learning with time series. Self-supervised learning, popular for learning intrinsic information from unlabeled data, has been adapted for contrastive learning in the computer vision domain [19,20,21,22,23,11]. Some works have applied contrastive learning to time series [14,24,25], such as TS2Vec [26], TS-TCC [27], and data augmentation schemes with mixing components [28]. Zhang et al. introduced a self-supervised pre-training strategy for time series, modeling Time-Frequency Consistency (TF-C) [29], while Khosla et al. extended self-supervised methods to fully supervised approaches, leveraging emotion label information in EEG samples [30].

Semi-supervised contrastive learning Semi-supervised learning has been integrated with contrastive learning for its ability to train networks with limited labeled data and large-scale unlabeled data [31,32,33]. Yang et al. proposed CCSSL to improve pseudo-label quality [34]; Singh et al. presented a temporal contrastive learning (TCL) framework for semi-supervised action recognition [35] and later proposed a simple Contrastive Learning framework for semi-supervised Domain Adaptation (CLDA) [36]; Kim et al. introduced SelfMatch, combining contrastive self-supervised learning and consistency regularization [37]; Inoue et al. proposed a semi-supervised contrastive learning framework based on generalized contrastive loss (GCL), unifying supervised metric learning and unsupervised contrastive learning [38].

End-to-end contrastive framework for time series. In contrastive learning, including self-supervised and the majority of semi-supervised methods, the two-stage framework is mainstream, involving a self-supervised pre-training stage followed by a supervised fine-tuning stage [27,39,40,41]. In many studies, when researchers refer to "semi-supervised contrastive" learning, they often mean that the overall two-stage framework utilizes both labeled and unlabeled samples. Although the entire model is considered semi-supervised, the pre-training stage remains unsupervised, as it primarily focuses on learning representations from unlabeled data. The two-stage framework has certain limitations (Section 1), which has led us to explore end-to-end solutions. Notably, there are several pioneering works in developing end-to-end models within the context of contrastive learning. Li et al. proposed an EEG-based emotion recognition method based on an efficient end-to-end CNN and contrastive learning (ECNN-C) [15]. They evaluated their models on two common EEG emotion datasets, DEAP [18] and DREAMER [42], demonstrating that the end-to-end network achieves high accuracy in time series classification. Furthermore, Zhang et al. [43] introduced a novel training strategy called Semi-supervised Contrastive Learning (SsCL), which combines the well-known contrastive loss in self-supervised learning with the cross-entropy loss in semi-supervised learning.

Nevertheless, ECNN-C solely relies on supervised learning, which requires a sufficient number of labeled samples and lacks plug-in compatibility. On the other hand, SsCL focuses on leveraging pseudo-labels and seeks an optimal approach to identify suitable positive pairs among all samples. Since the input data and problem definitions differ from ours, we do not directly compare our method with theirs in the experiments.

In this paper, we present a novel semi-supervised framework that achieves optimal performance with minimal labeled samples and can be seamlessly integrated into various architectures. Our approach systematically combines unsupervised contrastive loss, supervised contrastive loss, and classification loss to jointly update the model, maximizing the utilization of information from the data.

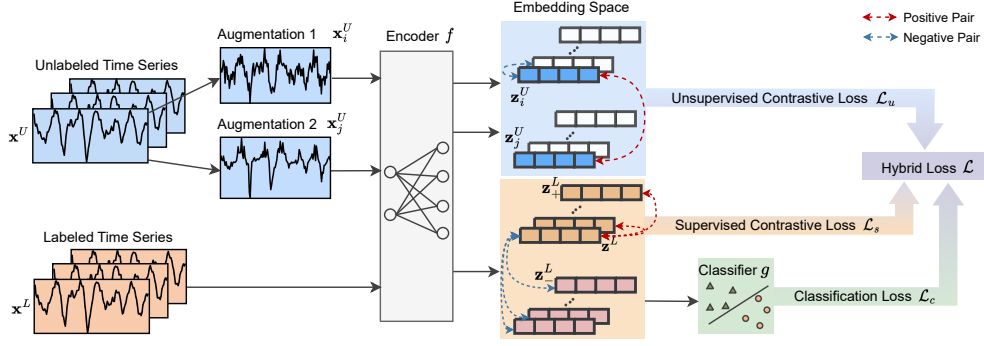


Figure 2: Overview of the proposed SLOTS. Our end-to-end model accepts a semi-labeled dataset consisting of unlabeled time series and labeled time series samples. We perform augmentations on the unlabeled sample x^U , generating two views x_i^U and x_j^U . These two views are fed into an encoder f that maps samples to a latent embedding space, where we compute the unsupervised contrastive loss \mathcal{L}_u through instance discrimination. Concurrently, we evaluate the supervised loss \mathcal{L}_s on the representations learned from the labeled sample x^L . The z_+^L associates with the same label as z^L while z_-^L belongs to a different label. Additionally, we calculate the classification loss \mathcal{L}_c on the labeled samples. The model is optimized using a hybrid loss \mathcal{L} .

3 Method

3.1 Problem Formulation

Suppose a semi-labelled time series dataset \mathcal{D} contains two parts: the unlabeled subset \mathcal{D}^U with N unlabeled sample x^U , and the labeled subset \mathcal{D}^L with M labeled sample x^L which associates with a label $y \in \{1, \dots, C\}$. The C denotes the number of classes. We denote the set of all available labels in \mathcal{D} as \mathcal{Y} . Without loss of generality, in the following descriptions, we focus on univariate (single-channel) time series x^U or x^L , while noting that our approach can accommodate multivariate time series of varying lengths across datasets.

Let f be the encoder that maps a time series sample to its representation in the latent space, and let g be the classifier that maps the latent representation to the class probabilities. **We aim to learn the optimal encoder f^* and classifier g^* by minimizing the following hybrid loss:**

$$(f^*, g^*) = \arg \min_{f, g} \left[\lambda_1 \mathcal{L}_u(f, \mathcal{D}^U) + \lambda_2 \mathcal{L}_s(f, \mathcal{D}^L, \mathcal{Y}) + \lambda_3 \mathcal{L}_c(f, g, \mathcal{D}^L, \mathcal{Y}) \right], \quad (1)$$

where $\mathcal{L}_u(f, \mathcal{D}^U)$ is the unsupervised contrastive loss, $\mathcal{L}_s(f, \mathcal{D}^L, \mathcal{Y})$ is the supervised contrastive loss, $\mathcal{L}_c(f, g, \mathcal{D}^L, \mathcal{Y})$ is the classification loss, and λ_1 , λ_2 , and λ_3 are the hyperparameters that balance the contributions of the three losses. The successful f^* and g^* can accurately predict the label for a new time series sample.

3.2 Model Architecture

We present the model pipeline of the proposed SLOTS in Figure 2. SLOTS receives a semi-labeled dataset \mathcal{D} , including an unlabeled subset \mathcal{D}^U and a labeled subset \mathcal{D}^L .

For each unlabeled sample $x^U \in \mathcal{D}^U$, SLOTS first generates two augmented views x_i^U and x_j^U using data augmentation techniques, such as jittering [27] and timestamp masking [26]. We use the subscripts i and j to mark the augmented samples. Then, these two augmented views are passed through the encoder $f(\cdot)$, resulting in their corresponding latent representations:

$$z_i^U = f(x_i^U), \quad z_j^U = f(x_j^U). \quad (2)$$

We calculate the unsupervised contrastive loss $\mathcal{L}_u(f, \mathcal{D}^U)$ in this embedding space. The z_i^U and z_j^U constructs a positive pair as they originated from the same input sample x^U ; in contrast, the embedding derived from different samples are regarded as negative pairs. Our preliminary results suggest a project header is not necessary in SLOTS.

For each labeled time series $x^L \in \mathcal{D}^L$, SLOTS directly sends it to the encoder f to learn the representation z^L through:

$$z^L = f(x^L). \quad (3)$$

The unlabeled sample x^U and labeled sample x^L are from the same original signal space and are mapped by the same encoder f . Therefore, we assume that the embeddings z_i^U , z_j^U , and z^L are located in the same latent space. In this space, we measure the supervised loss $\mathcal{L}_s(f, \mathcal{D}^L, \mathcal{Y})$. We assume that samples associated with the same label form positive pairs, while others form negative pairs. See more details of loss functions in Section 3.3.

Next, the representation z^L is fed into a classifier g , which produces the estimated sample label $\hat{y} = g(z^L)$. With the ground truth $y \in \mathcal{Y}$, we measure the classification loss $\mathcal{L}_c(f, g, \mathcal{D}^L, \mathcal{Y})$.

3.3 Semi-Supervised Contrastive Loss

Unsupervised contrastive loss. The unsupervised contrastive loss $\mathcal{L}_u(f, \mathcal{D}^U)$ aims to encourage the model to learn meaningful latent representations by minimizing the distance between the embeddings of augmented views of the same unlabeled sample, while maximizing the distance between the embeddings of different samples in the latent space. We leverage the contrastive learning framework and adopt the normalized temperature-scaled cross-entropy loss [11] for this purpose.

For each unlabeled sample $x^U \in \mathcal{D}^U$, we generate two augmented views x_i^U and x_j^U . After passing them through the encoder f , we obtain their corresponding embeddings z_i^U and z_j^U . The unsupervised contrastive loss, averaging across all samples, is computed as:

$$\mathcal{L}_u(f, \mathcal{D}^U) = \frac{1}{N} \sum_{i=1}^N -\log \frac{\exp(\text{sim}(z_i^U, z_j^U)/\tau)}{\sum_{k=1, k \neq i}^N \exp(\text{sim}(z_i^U, z_k^U)/\tau)}, \quad (4)$$

where sim is a similarity function (e.g., cosine similarity), τ is a temperature hyperparameter. By minimizing the unsupervised contrastive loss, the model learns to generate similar representations for augmented views of the same sample, while generating dissimilar representations for different samples in the latent space, which helps the model learn useful features from the unlabeled data.

Supervised contrastive loss. The supervised contrastive loss $\mathcal{L}_s(f, \mathcal{D}^L, \mathcal{Y})$ forces the model to learn discriminative features for labeled samples by maximizing the similarity between the representations of samples that belong to the same class while minimizing the similarity between the representations of samples from different classes. Compared to unsupervised loss, this is stronger guidance because true sample labels are directly involved as supervision.

Given a labeled time series $x^L \in \mathcal{D}^L$ with its corresponding ground truth label $y \in \mathcal{Y}$. We measure the supervised contrastive loss based on representation z^L :

$$\mathcal{L}_s(f, \mathcal{D}^L, \mathcal{Y}) = -\log \frac{\sum_{y=y_+} \exp(\text{sim}(z^L, z_+^L)/\tau)}{\sum_{y \neq y_-} \exp(\text{sim}(z^L, z_-^L)/\tau)}. \quad (5)$$

The z_+^L is a representation derived from a sample that belongs to the same class as z^L , i.e., $y = y_+$. Conversely, z_-^L is derived from a sample with a different label, such that $y \neq y_-$. Minimizing the supervised contrastive loss $\mathcal{L}_s(f, \mathcal{D}^L, \mathcal{Y})$ enables the model to produce more closely related representations for labeled samples belonging to the same class, while generating more distinct representations for labeled samples from different classes. This process promotes the learning of discriminative features that are beneficial for the classification task.

Classification loss. We incorporate a classification loss to directly optimize the model toward the classification task. We use the softmax cross-entropy loss, which is a widely used loss function for multi-class classification problems.

Given a labeled sample x^L , we obtain its predicted class probabilities $\hat{\mathbf{y}} = g(f(x^L))$. Let \hat{y}_c denote the predicted probability of class $c \in \{1, \dots, C\}$ for a given labeled sample. We calculate the classification loss between predicted class probabilities $\hat{\mathbf{y}}$ and the ground-truth labels \mathbf{y} :

$$\mathcal{L}_c(f, g, \mathcal{D}^L, \mathcal{Y}) = -\frac{1}{M} \sum_{i=1}^M \sum_{c=1}^C \mathbb{1}(y_i = c) \log \hat{y}_c, \quad (6)$$

where $\mathbb{1}(y_i = c)$ is an indicator function that equals 1 when the true label of the i -th labeled sample is c , and 0 otherwise. This loss directly optimizes the model for predicting the correct class labels.

Hybrid loss. The proposed end-to-end SLOTS is trained by jointly minimizing a hybrid loss \mathcal{L} , which is a weighted sum of the unsupervised contrastive loss, supervised contrastive loss, and classification loss, as described in the problem formulation (Equation 1). The three loss functions complement each other in terms of improving the classification results. During training, we update the encoder f and classifier g by minimizing the hybrid loss. This enables the model to learn effective representations from both unlabeled and labeled samples, while simultaneously improving its classification performance by directly optimizing the predicted class probabilities. The end-to-end training process allows the model to adaptively balance the contributions of the unsupervised, supervised, and classification losses to achieve the best performance on the given task.

4 Experiments

Datasets. (1) **DEAP**, a multimodal dataset based on the stimulation of music video materials, is used to analyze human emotional states [18]. It contains 32 subjects monitored by 32-channel EEG signals while watching 40 minutes (each minute is a trail) of videos. (2) **SEED** includes 62-channel EEG data of 15 subjects when they are watching 15 film clips with three types of emotions [44]. (3) **EPILEPSY** monitors the brain activities of 500 subjects with a single-channel EEG sensor (174 Hz) [45]. Each sample is labeled in binary based on whether the subject has epilepsy or not. (4) **HAR** has 10,299 9-dimension samples from 6 daily activities [46]. (5) **P19** (PhysioNet Sepsis Early Prediction Challenge 2019) includes 38,803 patients that are monitored by 34 sensors in ICU [47]. More dataset details are in Appendix A.

Baselines. We evaluate our SLOTS model by comparing it with ten baselines, consisting of five state-of-the-art contrastive methods that employ a two-stage framework and their improved end-to-end variants. The five state-of-the-art methods include TS2vec [26], Mixing-up [28], TS-TCC [27], SimCLR [11], and TFC [29]. To ensure a fair comparison, we create a two-stage version of SLOTS, named *SLOTS (two-stage)*, which can be directly compared with the five basic baselines. In addition, to adapt these baselines to our end-to-end framework, we modify the baselines and denote the updated versions with a ‘++’, resulting in a total of ten baselines. For instance, the end-to-end version of TS2Vec is referred to as TS2Vec++. In this paper, **unless explicitly stated otherwise, SLOTS refers to the SLOTS (end-to-end) model.**

Implementation. We adopt a dilated convolutional block as backbone for encoder f following [26]. A dilated module with three blocks is designed based on separable convolution. Each block consists of four distinct convolutional layers. The first layer employs a 2D convolution with a 1×1 kernel. The second and third layers utilize kernels of size 1×3 and 3×1 , respectively, replacing the 3×3 kernel in a manner similar to the MobileNet model. This reduces the number of parameters by 33% [48], enabling the network to operate more efficiently. The fourth layer is a spatial convolution with a depth multiplier of 2, doubling the number of channels from the first deep convolution layer. This layer allows the model to have sufficient channels to employ a reduction factor in bottleneck structures [49]. The classifier model g utilizes a linear fully connected layer with a single hidden unit as its structure. We employ temporal masking for time series augmentations. See more details of experimental settings (e.g., hardware, baseline details, and hyper-parameters) in Appendix B.

4.1 Comparing Frameworks: End-to-End versus Two-Stage

Table 1 presents the performance on the DEAP dataset in a leave-trials-out setting with labeling ratios ranging from 10% to 80%. Each baseline with the ‘++’ suffix is trained in an end-to-end framework. Here, we provide a detailed analysis of the results in terms of the absolute values of the F1 score. (1) The results demonstrate that transitioning a model from a two-stage to its end-to-end version (without any other changes) leads to significant performance improvement. For instance, at an 80% label ratio, TFC++ achieves the highest improvement over TFC, with a 20.13% increase. (2) Furthermore, our end-to-end SLOTS model consistently outmatches its two-stage counterpart, and the performance margin increases as the labeling ratio increases. Specifically, with 100% labeled data, SLOTS (end-to-end) achieved a significant improvement of 16.63% over SLOTS (two-stage).

Table 1: Performance comparison on DEAP dataset while the label ratio (the proportion of labeled samples in the training dataset) ranging from 10% to 100%.

Ratio	Models	Accuracy	Precision	Recall	F1 Score	AUROC	AUPRC
10%	TS2Vec	0.5125±0.0149	0.5020±0.0158	0.5029±0.2001	0.5002±0.0196	0.5200±0.0059	0.5365±0.0067
	TS2Vec++	0.5218±0.0123	0.5109±0.0214	0.5100±0.0211	0.5057±0.0236	0.5447±0.0146	0.5590±0.0125
	SimCLR	0.5150±0.0123	0.5173±0.0145	0.5154±0.0169	0.5096±0.0169	0.5194±0.0156	0.5292±0.0154
	SimCLR++	0.5862±0.0415	0.5912±0.0472	0.5848±0.0352	0.5716±0.0316	0.5874±0.0312	0.5815±0.0296
	TFC	0.5006±0.0152	0.5167±0.0254	0.5255±0.0356	0.5249±0.0445	0.5099±0.0365	0.5102±0.0421
	TFC++	0.6605±0.0547	0.6549±0.0365	0.6533±0.0542	0.6504±0.0654	0.7069±0.0412	0.7084±0.0357
	TS-TCC	0.5025±0.0631	0.4977±0.0614	0.4992±0.0748	0.4946±0.0861	0.5344±0.0743	0.5485±0.0763
	TS-TCC++	0.5547±0.0367	0.5431±0.0378	0.5409±0.0369	0.5358±0.0412	0.5575±0.0347	0.5680±0.0360
	MixingUp	0.5250±0.0165	0.5357±0.0162	0.5326±0.0198	0.5075±0.0186	0.5447±0.0164	0.5478±0.0157
	MixingUp++	0.6037±0.0974	0.5806±0.0874	0.6025±0.0962	0.5463±0.0871	0.6704±0.0634	0.6713±0.0631
	SLOTS (two-stage)	0.6276±0.0541	0.6393±0.0495	0.6138±0.0547	0.6055±0.0563	0.6704±0.0471	0.6480±0.0396
	SLOTS (end-to-end)	0.6636±0.0763	0.6598±0.0791	0.6571±0.0773	0.6556±0.0781	0.7115±0.0995	0.7118±0.0953
20%	TS2Vec	0.5250±0.0205	0.5397±0.0231	0.5308±0.0264	0.5004±0.0213	0.5361±0.0064	0.5452±0.0063
	TS2Vec++	0.5754±0.0096	0.6076±0.0068	0.5876±0.0067	0.5346±0.0099	0.6470±0.0037	0.6517±0.0048
	SimCLR	0.5225±0.0223	0.5199±0.0248	0.5168±0.0296	0.5128±0.0284	0.5235±0.0198	0.5412±0.0196
	SimCLR++	0.6061±0.0521	0.6078±0.0543	0.5928±0.0469	0.5855±0.0437	0.6376±0.0379	0.6355±0.0380
	TFC	0.5375±0.0084	0.5326±0.0099	0.5321±0.0152	0.5316±0.0251	0.5123±0.0325	0.5315±0.0241
	TFC++	0.6896±0.0420	0.6855±0.0254	0.6833±0.0421	0.6784±0.0362	0.7384±0.0125	0.7405±0.0152
	TS-TCC	0.5105±0.0459	0.5137±0.0423	0.5228±0.0479	0.5105±0.0523	0.6006±0.0418	0.6000±0.0412
	TS-TCC++	0.5613±0.0412	0.5614±0.0430	0.5540±0.0426	0.5442±0.0497	0.5714±0.0409	0.5804±0.0410
	MixingUp	0.5281±0.0089	0.5531±0.0110	0.5436±0.0102	0.5083±0.0163	0.5692±0.0165	0.5704±0.0135
	MixingUp++	0.6418±0.0861	0.6696±0.0845	0.6309±0.0960	0.5954±0.0934	0.7119±0.0847	0.7109±0.0823
	SLOTS (two-stage)	0.6699±0.0452	0.6577±0.0432	0.6541±0.0632	0.6171±0.0542	0.6877±0.0512	0.6954±0.0510
	SLOTS (end-to-end)	0.7618±0.0954	0.7599±0.0894	0.7563±0.0942	0.7553±0.0875	0.8155±0.0644	0.8164±0.0497
40%	TS2Vec	0.5300±0.0231	0.5423±0.0247	0.5376±0.0239	0.5193±0.0267	0.5367±0.0146	0.5478±0.0176
	TS2Vec++	0.6169±0.0563	0.6587±0.0542	0.6011±0.0641	0.5697±0.0678	0.6939±0.0541	0.6963±0.0512
	SimCLR	0.5325±0.0224	0.5283±0.0236	0.5290±0.0245	0.5216±0.0278	0.5367±0.0214	0.5469±0.0228
	SimCLR++	0.6106±0.0254	0.6385±0.0247	0.6115±0.0279	0.5914±0.0341	0.6836±0.0316	0.6842±0.0341
	TFC	0.5500±0.0063	0.5533±0.0054	0.5500±0.0072	0.5429±0.0077	0.5850±0.0033	0.5926±0.0026
	TFC++	0.7367±0.0235	0.7333±0.0351	0.7304±0.0369	0.7274±0.0452	0.7857±0.0357	0.7913±0.0347
	TS-TCC	0.5525±0.0196	0.5288±0.0213	0.5308±0.0236	0.5183±0.0255	0.6032±0.0194	0.6016±0.0184
	TS-TCC++	0.6021±0.0239	0.5991±0.0241	0.5883±0.0310	0.5768±0.0334	0.6320±0.0229	0.6332±0.0263
	MixingUp	0.5781±0.0561	0.5924±0.0515	0.5850±0.0498	0.5553±0.0698	0.6085±0.0244	0.6176±0.0255
	MixingUp++	0.6479±0.0645	0.7101±0.0633	0.6653±0.0542	0.6211±0.0655	0.7730±0.0365	0.7707±0.0365
	SLOTS (two-stage)	0.6742±0.3254	0.6797±0.0412	0.6637±0.0523	0.6701±0.0489	0.7087±0.0421	0.7114±0.0432
	SLOTS (end-to-end)	0.8299±0.0542	0.8281±0.0499	0.8268±0.0621	0.8255±0.0634	0.8757±0.0510	0.8766±0.0515
60%	TS2Vec	0.5312±0.0198	0.5486±0.0174	0.5378±0.0234	0.5233±0.0249	0.5479±0.0132	0.5518±0.0126
	TS2Vec++	0.6573±0.0525	0.6773±0.0547	0.6397±0.0519	0.6287±0.0643	0.7282±0.0532	0.7301±0.0531
	SimCLR	0.5375±0.0361	0.5307±0.0348	0.5262±0.0396	0.5179±0.0454	0.5393±0.0362	0.5464±0.0352
	SimCLR++	0.6396±0.0351	0.6561±0.0335	0.6452±0.0417	0.6299±0.0456	0.7052±0.0413	0.7062±0.0415
	TFC	0.5875±0.0126	0.5922±0.0263	0.5875±0.0231	0.5822±0.0237	0.6119±0.0322	0.6025±0.0324
	TFC++	0.7647±0.0668	0.7616±0.0574	0.7595±0.0741	0.7585±0.0596	0.8150±0.0614	0.8224±0.0532
	TS-TCC	0.5625±0.0346	0.5663±0.0348	0.5611±0.0417	0.5413±0.0454	0.6091±0.0346	0.6027±0.0333
	TS-TCC++	0.6026±0.0333	0.6058±0.0341	0.5900±0.0387	0.5792±0.0410	0.6404±0.0332	0.6413±0.0335
	MixingUp	0.6062±0.0868	0.6437±0.0844	0.6074±0.0725	0.6011±0.0769	0.6159±0.0631	0.6199±0.0612
	MixingUp++	0.6960±0.0621	0.7304±0.0555	0.6731±0.0635	0.6392±0.0789	0.7837±0.0541	0.7845±0.0569
	SLOTS (two-stage)	0.7054±0.0535	0.7038±0.0478	0.7275±0.0621	0.6975±0.0598	0.7610±0.0459	0.7564±0.0425
	SLOTS (end-to-end)	0.8728±0.0625	0.8719±0.0654	0.8703±0.0968	0.8696±0.0842	0.9101±0.0682	0.9112±0.0574
80%	TS2Vec	0.5475±0.0213	0.5368±0.0241	0.5355±0.0219	0.5341±0.0238	0.5491±0.0196	0.5549±0.0194
	TS2Vec++	0.6886±0.0436	0.7112±0.0479	0.6672±0.0521	0.6587±0.0642	0.7704±0.0534	0.7691±0.0537
	SimCLR	0.5400±0.0169	0.5677±0.0198	0.5640±0.0246	0.5383±0.0234	0.5365±0.0167	0.5457±0.0165
	SimCLR++	0.6958±0.0517	0.6994±0.0514	0.6847±0.0496	0.6823±0.0463	0.7641±0.0521	0.7575±0.0530
	TFC	0.6025±0.0168	0.6048±0.0167	0.5918±0.0215	0.5926±0.0266	0.6212±0.0214	0.6470±0.0215
	TFC++	0.8000±0.0354	0.7967±0.0471	0.7953±0.0532	0.7939±0.0613	0.8403±0.0536	0.8459±0.0475
	TS-TCC	0.5675±0.0310	0.5701±0.0296	0.5697±0.0309	0.5529±0.0342	0.6115±0.0296	0.6092±0.0284
	TS-TCC++	0.6028±0.0298	0.6077±0.0310	0.5933±0.0301	0.5889±0.0364	0.6492±0.0263	0.6420±0.0254
	MixingUp	0.6500±0.0551	0.6540±0.0351	0.6529±0.0532	0.6498±0.0647	0.6679±0.0345	0.6547±0.0367
	MixingUp++	0.6973±0.0542	0.7443±0.0596	0.6804±0.0496	0.6522±0.0515	0.8091±0.0362	0.8090±0.0337
	SLOTS (two-stage)	0.7312±0.0625	0.7460±0.0654	0.7520±0.0741	0.7615±0.0632	0.7812±0.0678	0.8210±0.0593
	SLOTS (end-to-end)	0.9037±0.0774	0.9028±0.0710	0.9028±0.0821	0.9020±0.0736	0.9282±0.0630	0.9294±0.0622
100%	TS2Vec	0.5499±0.0225	0.5373±0.0172	0.5376±0.0200	0.5478±0.0235	0.5597±0.0046	0.5788±0.0050
	TS2Vec++	0.6982±0.0720	0.7160±0.0716	0.6684±0.0718	0.6629±0.0726	0.7726±0.0912	0.7810±0.0866
	SimCLR	0.5687±0.0212	0.5728±0.0235	0.5682±0.0194	0.5460±0.0198	0.5694±0.0157	0.5524±0.0096
	SimCLR++	0.7087±0.0412	0.7028±0.0455	0.6882±0.0494	0.6860±0.0497	0.7694±0.0453	0.7594±0.0481
	TFC	0.6225±0.0025	0.6181±0.0065	0.6475±0.0043	0.6037±0.0047	0.6538±0.0191	0.6513±0.0223
	TFC++	0.8167±0.0914	0.8074±0.0902	0.8125±0.0958	0.8118±0.0959	0.8504±0.0772	0.8526±0.0750
	TS-TCC	0.5725±0.0150	0.5706±0.0171	0.5713±0.0119	0.5558±0.0065	0.6185±0.0014	0.6161±0.0056
	TS-TCC++	0.6184±0.0292	0.6209±0.0371	0.5996±0.0239	0.5897±0.0226	0.6606±0.0474	0.6610±0.0439
	MixingUp	0.6562±0.0062	0.6610±0.0082	0.6504±0.0033	0.6505±0.0154	0.6717±0.0364	0.6852±0.0271
	MixingUp++	0.7499±0.1017	0.7576±0.1037	0.7430±0.1036	0.7372±0.1112	0.7050±0.0924	0.7048±0.0926
	SLOTS (two-stage)	0.7525±0.0500	0.7594±0.0585	0.7401±0.0398	0.7664±0.0415	0.8197±0.0067	0.8388±0.0087
	SLOTS (end-to-end)	0.9342±0.1161	0.9329±0.1171	0.9335±0.1184	0.9327±0.1187	0.9456±0.0966	0.9469±0.0952

Table 2: Performance comparison on SEED, P19, EPILEPSY, and HAR, under the label ratio of 10%. To save space, we show the extended table with errorbars in Appendix C.

Models	SEED						P19					
	Accuracy	Precision	Recall	F1 score	AUROC	AUPRC	Accuracy	Precision	Recall	F1 score	AUROC	AUPRC
TS2Vec	0.5750	0.6048	0.5732	0.5113	0.6493	0.6218	0.6580	0.6467	0.5520	0.5669	0.5171	0.5860
TS2Vec++	0.6252	0.6191	0.6084	0.5599	0.6607	0.6962	0.6589	0.6794	0.6500	0.6894	0.6527	0.6978
TS-TCC	0.5893	0.5627	0.5772	0.5723	0.7137	0.6941	0.9216	0.5968	0.6597	0.6156	0.6941	0.6667
TS-TCC++	0.6172	0.5935	0.5776	0.5977	0.8004	0.7637	0.9654	0.7338	0.6776	0.7076	0.7011	0.7065
SimCLR	0.5050	0.5115	0.5313	0.5155	0.6963	0.6982	0.9130	0.5877	0.5600	0.5338	0.5995	0.5956
SimCLR++	0.5736	0.5344	0.5505	0.5374	0.6802	0.6361	0.9534	0.6924	0.6124	0.6321	0.7077	0.6554
MixingUp	0.5166	0.5356	0.5638	0.5141	0.6605	0.6580	0.9136	0.6744	0.6481	0.6477	0.6802	0.6361
MixingUp++	0.5569	0.5701	0.5638	0.5265	0.7494	0.6603	0.9253	0.6777	0.6500	0.6489	0.7685	0.6932
TFC	0.5500	0.5356	0.5487	0.5290	0.7499	0.6423	0.9049	0.6207	0.6340	0.6267	0.6399	0.7092
TFC++	0.6087	0.6121	0.6071	0.5990	0.7847	0.6685	0.9361	0.7500	0.6761	0.6954	0.7721	0.7287
SLOTS (two-stage)	0.6468	0.6573	0.7316	0.6169	0.7575	0.7572	0.9254	0.7138	0.6776	0.7076	0.7011	0.7065
SLOTS (end-to-end)	0.7181	0.7286	0.7869	0.6510	0.8034	0.7592	0.9596	0.7580	0.7416	0.7788	0.7703	0.8270

Models	EPILEPSY					HAR						
	Accuracy	Precision	Recall	F1 score	AUROC	AUPRC	Accuracy	Precision	Recall	F1 score	AUROC	AUPRC
TS2Vec	0.5125	0.5604	0.5118	0.5287	0.6519	0.6233	0.5738	0.5555	0.5768	0.5565	0.7623	0.7413
TS2Vec++	0.6022	0.6011	0.5500	0.5445	0.6537	0.6498	0.6743	0.6197	0.5838	0.5701	0.8488	0.8114
TS-TCC	0.6175	0.6338	0.5000	0.5403	0.6029	0.6726	0.6596	0.6154	0.6158	0.5459	0.7511	0.7414
TS-TCC++	0.6206	0.6401	0.5459	0.5445	0.6851	0.7150	0.6787	0.6473	0.6316	0.6169	0.7575	0.7572
SimCLR	0.6375	0.5938	0.5200	0.5100	0.6293	0.6776	0.6168	0.6390	0.5704	0.5744	0.7452	0.7098
SimCLR++	0.6805	0.6591	0.5084	0.5599	0.6607	0.6962	0.6217	0.6435	0.6205	0.5977	0.9004	0.7637
MixingUp	0.6175	0.6115	0.5313	0.5485	0.6596	0.6782	0.6277	0.6393	0.6138	0.6055	0.7705	0.7481
MixingUp++	0.6617	0.6356	0.5804	0.5734	0.6605	0.6980	0.6699	0.6577	0.6541	0.6172	0.8878	0.8254
TFC	0.6550	0.6312	0.5250	0.5226	0.5390	0.6653	0.6502	0.6102	0.6083	0.6095	0.7315	0.7371
TFC++	0.6693	0.6627	0.5472	0.5472	0.7014	0.6834	0.7263	0.6479	0.6634	0.6512	0.8519	0.8064
SLOTS (two-stage)	0.6652	0.6591	0.5684	0.5599	0.6607	0.6962	0.6654	0.6538	0.6276	0.6076	0.8011	0.7565
SLOTS (end-to-end)	0.6955	0.6952	0.5999	0.5819	0.7105	0.7600	0.7312	0.6661	0.6720	0.6615	0.9013	0.8811

Table 3: Ablation study (DEAP; 10% label ratio). ‘W/o \mathcal{L}_u ’ means removing unsupervised contrastive loss, i.e., encoders and classifiers are updated with supervised loss and cross-entropy loss. ‘W/o \mathcal{L}_s ’ refers to removing supervised contrastive loss, i.e., encoders and classifiers are updated with unsupervised loss and classification loss. ‘W/ \mathcal{L}_s ’ refers to introducing supervised contrastive loss in SLOTS’s fine-tuning stage.

Models	Methods	Accuracy	Precision	Recall	F1 score	AUROC	AUPRC
SLOTS (two-stage)	W/ \mathcal{L}_s in fine-tuning	0.6375 \pm 0.0100	0.6433 \pm 0.0255	0.6359 \pm 0.0130	0.6308 \pm 0.0159	0.6897 \pm 0.0061	0.6865 \pm 0.0067
	Full model	0.6276 \pm 0.0541	0.6393 \pm 0.0495	0.6138 \pm 0.0547	0.6055 \pm 0.0563	0.6704 \pm 0.0471	0.6480 \pm 0.0396
SLOTS (end-to-end)	W/o \mathcal{L}_u	0.6590 \pm 0.0724	0.6548 \pm 0.0757	0.6490 \pm 0.0736	0.6472 \pm 0.0748	0.7042 \pm 0.0961	0.7049 \pm 0.0927
	W/o \mathcal{L}_s	0.6103 \pm 0.0520	0.6072 \pm 0.0583	0.5953 \pm 0.0497	0.5905 \pm 0.0495	0.6438 \pm 0.0771	0.6469 \pm 0.0714
	Full model	0.6636\pm0.0763	0.6598\pm0.0791	0.6571\pm0.0773	0.6556\pm0.0781	0.7115\pm0.0995	0.7118\pm0.0953

4.2 Comparing Model: SLOTS versus Baselines

Our end-to-end SLOTS model consistently outperforms all ten baselines. With a full availability of data labels, SLOTS (end-to-end) achieves the highest performance of 93.27%, surpassing the best baseline, TFC++ (81.18%), by a significant margin of 12.09% (Table 1). Additionally, our model outperforms all baselines across multiple datasets, including SEED, P19, EPILEPSY, and HAR datasets (Table 2). Overall, our SLOTS (end-to-end) model achieves victory in 21 out of 24 tests (6 metrics in 4 datasets) and is the second-best performer in 3 other tests.

Ablation study To demonstrate the importance of each loss component, we examine two scenarios: 1) removing unsupervised losses; 2) removing supervised losses. Both scenarios result in degraded performance (DEAP; 10% labeling ratio; Table 3)). Additionally, we incorporate a supervised contrastive loss into the two-stage version of SLOTS, which leads to a slight increase (1% in accuracy) but still remains 2.6% lower than the end-to-end framework.

4.3 Robustness Across Trials and Subjects

Taking emotion recognition (DEAP; 40% labels) as an example, we investigate the robustness of SLOTS in three settings (Appendix D): trial-dependent, leave-trials-out, and leave-subjects-out. We compare SLOTS with MixingUp which is the strongest baseline on DEAP (Table 1). In Table 4, as expected, the trial-dependent pattern outstrips leave-trials-out, which in turn outperforms the leave-subjects-out pattern. This could be due to inter-trial and inter-subject variations [14]. In the trial-dependent pattern, SLOTS (end-to-end) achieves the highest F1 score of 94.04%, surpassing MixingUp by 30.64% and MixingUp++ by 7.92%. SLOTS (end-to-end) consistently performs best across all three patterns and six metrics, demonstrating the effectiveness of SLOTS.

Table 4: Performance comparison (DEAP; 40% label ratio) across trial-dependent, leave-trials-out, and leave-subjects-out settings. We present the comparison with the strongest baseline on DEAP (MixingUp) to save space.

Patterns	Models	Accuracy	Precision	Recall	F1 Score	AUROC	AUPRC
Trial-dependent	MixingUp	0.6563 \pm 0.0012	0.6692 \pm 0.0065	0.6499 \pm 0.0111	0.6340 \pm 0.0047	0.7400 \pm 0.0058	0.7262 \pm 0.0052
	MixingUp++	0.8670 \pm 0.0738	0.8827 \pm 0.0638	0.8676 \pm 0.0698	0.8612 \pm 0.0777	0.9548 \pm 0.0371	0.9537 \pm 0.0371
	SLOTS (end-to-end)	0.9418\pm0.0279	0.9410\pm0.0280	0.9410\pm0.0287	0.9404\pm0.0286	0.9818\pm0.0134	0.9817\pm0.0132
Leave-trials-out	MixingUp	0.5781 \pm 0.0561	0.5924 \pm 0.0515	0.5850 \pm 0.0498	0.5553 \pm 0.0698	0.6085 \pm 0.0244	0.6176 \pm 0.0255
	MixingUp++	0.6479 \pm 0.0645	0.7101 \pm 0.0633	0.6653 \pm 0.0542	0.6211 \pm 0.0655	0.7730 \pm 0.0365	0.7707 \pm 0.0365
	SLOTS (end-to-end)	0.8299\pm0.0542	0.8281\pm0.0499	0.8268\pm0.0621	0.8255\pm0.0634	0.8757\pm0.0510	0.8766\pm0.0515
Leave-subjects-out	MixingUp	0.5062 \pm 0.0038	0.5202 \pm 0.0017	0.5186 \pm 0.0107	0.5104 \pm 0.0085	0.5878 \pm 0.0118	0.5891 \pm 0.0086
	MixingUp++	0.6085 \pm 0.0136	0.6640 \pm 0.0182	0.6278 \pm 0.0088	0.5788 \pm 0.0121	0.7010 \pm 0.0106	0.7006 \pm 0.0099
	SLOTS (end-to-end)	0.6765\pm0.1204	0.6864\pm0.1175	0.6818\pm0.1156	0.6708\pm0.1200	0.7330\pm0.1342	0.7365\pm0.1280

5 Discussion and Future Works

SLOTS demonstrated promising results across various datasets, outperforming ten competitive baselines. Nevertheless, there are several aspects that warrant further investigation and improvements.

Firstly, the methodology employed in our approach prioritizes enhanced performance at the expense of transferability. Unlike two-stage models that facilitate pre-training on a distinct dataset followed by fine-tuning on a smaller dataset, our end-to-end model necessitates that both pre-training and fine-tuning datasets be derived from the same source. This constraint hampers the model’s capacity to transfer knowledge across disparate tasks and datasets. A potential remedy to this issue may entail incorporating domain adaptation techniques, as delineated by Wilson et al. (2020) [50], to address both model performance and knowledge transferability concurrently.

Secondly, the existing model offers opportunities for extension to a wider array of downstream tasks. In principle, our end-to-end framework can be tailored to accommodate tasks such as clustering, forecasting, regression, anomaly detection, and other time series data tasks, granted that an appropriate task-specific loss function is incorporated.

Lastly, the data augmentation techniques employed in our model warrant further refinement [51]. The development of more sophisticated and task-specific augmentation methods could yield superior representations, consequently enhancing the model’s performance.

6 Conclusion

This paper presented SLOTS, an end-to-end model for semi-supervised time series classification, which combines unsupervised contrastive loss, supervised contrastive loss, and classification loss in a unified framework. The hybrid loss function effectively leverages both labeled and unlabeled data to learn discriminative features, while the end-to-end training process allows the model to adaptively balance the contributions of these losses to achieve optimal performance. Extensive experiments demonstrated that SLOTS surpasses state-of-the-art methods and their end-to-end adaptations, showcasing its effectiveness and versatility in handling time series classification tasks.

Broader Impacts. SLOTS can be seamlessly applied to broad applications, potentially enhancing decision-making and prediction capabilities. However, improper use or biases in training data may lead to unintended consequences and discriminatory outcomes, necessitating responsible deployment and ethical considerations. It is crucial to ensure the quality and fairness of the training data and establish guidelines for the responsible and transparent use of SLOTS in real-world applications.

References

- [1] Xilin Li. Convolutional PCA for multiple time series. *IEEE Signal Processing Letters*, 27:1450–1454, 2020.
- [2] Hrayr Harutyunyan, Hrant Khachatrian, David C Kale, Greg Ver Steeg, and Aram Galstyan. Multitask learning and benchmarking with clinical time series data. *Scientific data*, 6(1):1–18, 2019.

- [3] Shahbaz Rezaei and Xin Liu. Deep learning for encrypted traffic classification: An overview. *IEEE communications magazine*, 57(5):76–81, 2019.
- [4] Suman Ravuri, Karel Lenc, Matthew Willson, Dmitry Kangin, Remi Lam, Piotr Mirowski, Megan Fitzsimons, Maria Athanassiadou, Sheleem Kashem, Sam Madge, et al. Skilful precipitation nowcasting using deep generative models of radar. *Nature*, 597(7878):672–677, 2021.
- [5] Omer Berat Sezer, Mehmet Ugur Gudelek, and Ahmet Murat Ozbayoglu. Financial time series forecasting with deep learning: A systematic literature review: 2005–2019. *Applied soft computing*, 90:106181, 2020.
- [6] Bing Su and Jirong Wen. Temporal alignment prediction for supervised representation learning and few-shot sequence classification. In *ICLR*, pages 1–19, 2022.
- [7] Yixiang Deng, Lu Lu, Laura Aponte, Angeliki M. Angelidi, Vera Novak, George Em Karniadakis, and Christos S. Mantzoros. Deep transfer learning and data augmentation improve glucose levels prediction in type 2 diabetes patients. *NPJ Digital Medicine*, 4(1):1–13, 2021.
- [8] Mostafa Neo Mohsenvand, Mohammad Rasool Izadi, and Pattie Maes. Contrastive representation learning for electroencephalogram classification. In *Machine Learning for Health NeurIPS Workshop*, pages 238–253, 2020.
- [9] Yu Wang, Jingyang Lin, Qi Cai, Yingwei Pan, Ting Yao, Hongyang Chao, and Tao Mei. A low rank promoting prior for unsupervised contrastive learning. *IEEE Transactions on Pattern Analysis and Machine Intelligence*, 45(3):2667–2681, 2023.
- [10] Johannes Pöppelbaum, Gavneet Singh Chadha, and Andreas Schwung. Contrastive learning based self-supervised time-series analysis. *Applied Soft Computing*, 117:108397, 2022.
- [11] Ting Chen, Simon Kornblith, Mohammad Norouzi, and Geoffrey Hinton. A simple framework for contrastive learning of visual representations. In *ICML*, page 1597–1607, 2020.
- [12] Xue Jiang, Jianhui Zhao, Bo Du, and Zhiyong Yuan. Self-supervised contrastive learning for EEG-based sleep staging. In *International Joint Conference on Neural Networks*, pages 1–8, 2021.
- [13] Haoning Kan, Jiale Yu, Jiajin Huang, Zihui Liu, and Haiyan Zhou. Self-supervised group meiosis contrastive learning for EEG-based emotion recognition. *ArXiv*, abs/2208.00877:1–14, 2022.
- [14] Xinke Shen, Xianggen Liu, Xin Hu, Dan Zhang, and Sen Song. Contrastive learning of subject-invariant EEG representations for cross-subject emotion recognition. *IEEE Transactions on Affective Computing*, pages 1–17, 2022.
- [15] Chang Li, Xuejuan Lin, Yu Liu, Rencheng Song, Juan Cheng, and Xun Chen. EEG-based emotion recognition via efficient convolutional neural network and contrastive learning. *IEEE Sensors Journal*, 22(20):19608–19619, 2022.
- [16] Pilhyeon Lee, Sunhee Hwang, Jewook Lee, Minjung Shin, Seogkyu Jeon, and Hyeran Byun. Inter-subject contrastive learning for subject adaptive EEG-based visual recognition. In *International Winter Conference on Brain-Computer Interface*, pages 1–6, 2022.
- [17] Yang Li, Ji Chen, Fu Li, Boxun Fu, Hao Wu, Youshuo Ji, Yijin Zhou, Yi Niu, Guangming Shi, and Wenming Zheng. GMSS: Graph-based multi-task self-supervised learning for EEG emotion recognition. *IEEE Transactions on Affective Computing*, pages 1–15, 2022.
- [18] Sander Koelstra, Christian Muhl, Mohammad Soleymani, Jong-Seok Lee, Ashkan Yazdani, Touradj Ebrahimi, Thierry Pun, Anton Nijholt, and Ioannis Patras. Deap: A database for emotion analysis using physiological signals. *IEEE Transactions on Affective Computing*, 3(1):18–31, 2012.
- [19] Ishan Misra, C. Lawrence Zitnick, and Martial Hebert. Shuffle and learn: Unsupervised learning using temporal order verification. In *European Conference on Computer Vision*, pages 527–544, 2016.

- [20] Tomas Mikolov, Ilya Sutskever, Kai Chen, Greg Corrado, and Jeffrey Dean. Distributed representations of words and phrases and their compositionality. *NeurIPS*, 26:3111–3119, 2013.
- [21] Jacob Devlin, Mingwei Chang, Kenton Lee, and Kristina Toutanova. BERT: Pre-training of deep bidirectional transformers for language understanding. In *Conference of the North American Chapter of the Association for Computational Linguistics*, pages 4171–4186, 2019.
- [22] Phuc H. Le-Khac, Graham Healy, and Alan F. Smeaton. Contrastive representation learning: A framework and review. *IEEE Access*, 8:193907–193934, 2020.
- [23] Kaiming He, Haoqi Fan, Yuxin Wu, Saining Xie, and Ross Girshick. Momentum contrast for unsupervised visual representation learning. In *IEEE/CVF Conference on Computer Vision and Pattern Recognition*, pages 9726–9735, 2020.
- [24] Hubert Banville, Omar Chehab, Aapo Hyvärinen, Denis-Alexander Engemann, and Alexandre Gramfort. Uncovering the structure of clinical EEG signals with self-supervised learning. *Journal of Neural Engineering*, 18(4):046020, 2021.
- [25] Fu Li, Hongxin Li, Yang Li, Hao Wu, Boxun Fu, Youshuo Ji, Chong Wang, and Guangming Shi. Decoupling representation learning for imbalanced electroencephalography classification in rapid serial visual presentation task. *Journal of Neural Engineering*, 19(3):1–19, 2022.
- [26] Zhihan Yue, Yujing Wang, Juanyong Duan, Tianmeng Yang, Congrui Huang, Yunhai Tong, and Bixiong Xu. TS2Vec: Towards universal representation of time series. In *AAAI*, pages 8980–8987, 2022.
- [27] Emadeldeen Eldele, Mohamed Ragab, Zhenghua Chen, Min Wu, Chee Keong Kwoh, Xiaoli Li, and Cuntai Guan. Time-series representation learning via temporal and contextual contrasting. In *International Joint Conference on Artificial Intelligence*, pages 2352–2359, 2021.
- [28] Kristoffer Wickstrøm, Michael Kampffmeyer, Karl Øyvind Mikalsen, and Robert Jenssen. Mixing up contrastive learning: Self-supervised representation learning for time series. *Pattern Recognition Letters*, 155:54–61, 2022.
- [29] Xiang Zhang, Ziyuan Zhao, Theodoros Tsiligkaridis, and Marinka Zitnik. Self-supervised contrastive pre-training for time series via time-frequency consistency. In *NeurIPS*, pages 1–32, 2022.
- [30] Prannay Khosla, Piotr Teterwak, Chen Wang, Aaron Sarna, Yonglong Tian, Phillip Isola, Aaron Maschinot, Ce Liu, and Dilip Krishnan. Supervised contrastive learning. *NeurIPS*, 33:18661–18673, 2020.
- [31] Eric Arazo, Diego Ortego, Paul Albert, Noel E. O’Connor, and Kevin McGuinness. Pseudo-labeling and confirmation bias in deep semi-supervised learning. In *International Joint Conference on Neural Networks*, pages 1–8, 2020.
- [32] Takeru Miyato, Shin Ichi Maeda, Masanori Koyama, and Shin Ishii. Virtual adversarial training: A regularization method for supervised and semi-supervised learning. *IEEE Transactions on Pattern Analysis and Machine Intelligence*, 41(8):1979–1993, 2019.
- [33] Mehdi Sajjadi, Mehran Javanmardi, and Tolga Tasdizen. Regularization with stochastic transformations and perturbations for deep semi-supervised learning. In *Neural Information Processing Systems*, pages 1163–1171, 2016.
- [34] Fan Yang, Kai Wu, Shuyi Zhang, Guannan Jiang, Yong Liu, Feng Zheng, Wei Zhang, Chengjie Wang, and Long Zeng. Class-aware contrastive semi-supervised learning. In *IEEE/CVF CVPR*, pages 14421–14430, 2022.
- [35] Ankit Singh, Omprakash Chakraborty, Ashutosh Varshney, Rameswar Panda, Rogerio Feris, Kate Saenko, and Abir Das. Semi-supervised action recognition with temporal contrastive learning. In *IEEE/CVF CVPR*, pages 10384–10394, 2021.
- [36] Ankit Singh. CLDA: Contrastive learning for semi-supervised domain adaptation. In *NeurIPS*, pages 5089–5101, 2021.

- [37] Byoungjip Kim, Jinho Choo, Yeong-Dae Kwon, Seongho Joe, Seungjai Min, and Youngjune Gwon. Selfmatch: Combining contrastive self-supervision and consistency for semi-supervised learning. *arXiv*, 2101.06480:2021, 2021.
- [38] Nakamasa Inoue and Keita Goto. Semi-supervised contrastive learning with generalized contrastive loss and its application to speaker recognition. In *Asia-Pacific Signal and Information Processing Association Annual Summit and Conference*, pages 1641–1646, 2020.
- [39] Qinfeng Xiao, Jing Wang, Jianan Ye, Hongjun Zhang, Yuyan Bu, Yiqiong Zhang, and Hao Wu. Self-supervised learning for sleep stage classification with predictive and discriminative contrastive coding. In *IEEE International Conference on Acoustics, Speech and Signal Processing*, pages 1290–1294, 2021.
- [40] Xiaomin Li and Vangelis Metsis. SPP-EEGNET: An input-agnostic self-supervised EEG representation model for inter-dataset transfer learning. In *International Conference on Computing and Information Technology*, pages 173–182, 2022.
- [41] Demetres Kostas, Stéphane Aroca-Ouellette, and Frank Rudzicz. BENDR: Using transformers and a contrastive self-supervised learning task to learn from massive amounts of EEG data. *Frontiers in Human Neuroscience*, 15:1–15, 2021.
- [42] Stamos Katsigiannis and Naeem Ramzan. DREAMER: A database for emotion recognition through EEG and ECG signals from wireless low-cost off-the-shelf devices. *IEEE Journal of Biomedical and Health Informatics*, 22(1):98–107, 2018.
- [43] Yuhang Zhang, Xiaopeng Zhang, Jie Li, Robert Qiu, Haohang Xu, and Qi Tian. Semi-supervised contrastive learning with similarity co-calibration. *IEEE Transactions on Multimedia*, pages 1–11, 2022.
- [44] Weilong Zheng, Jiayi Zhu, and Baoliang Lu. Identifying stable patterns over time for emotion recognition from EEG. *IEEE Transactions on Affective Computing*, 10(3):417–429, 2019.
- [45] Ralph G Andrzejak, Klaus Lehnertz, Florian Mormann, Christoph Rieke, Peter David, and Christian E Elger. Indications of nonlinear deterministic and finite-dimensional structures in time series of brain electrical activity: Dependence on recording region and brain state. *Physical Review E*, 64(6):061907, 2001.
- [46] Davide Anguita, Alessandro Ghio, Luca Oneto, Xavier Parra Perez, and Jorge Luis Reyes Ortiz. A public domain dataset for human activity recognition using smartphones. In *European Symposium on Artificial Neural Networks, Computational Intelligence and Machine Learning*, pages 437–442, 2013.
- [47] Matthew A Reyna, Christopher S Josef, Russell Jeter, Supreeth P Shashikumar, M Brandon Westover, Shamim Nemati, Gari D Clifford, and Ashish Sharma. Early prediction of sepsis from clinical data: The physionet/computing in cardiology challenge 2019. *Critical Care Medicine*, 48(2):210–217, 2020.
- [48] Chang Li, Xuejuan Lin, Yu Liu, Rencheng Song, Juan Cheng, and Xun Chen. EEG-based emotion recognition via efficient convolutional neural network and contrastive learning. *IEEE Sensors Journal*, 22(20):19608–19619, 2022.
- [49] Ido Freeman, Lutz Roesse-Koerner, and Anton Kummert. Effnet: An efficient structure for convolutional neural networks. In *IEEE International Conference on Image Processing*, pages 6–10, 2018.
- [50] Garrett Wilson, Janardhan Rao Doppa, and Diane J Cook. Multi-source deep domain adaptation with weak supervision for time-series sensor data. In *SIGKDD*, pages 1768–1778, 2020.
- [51] Ziyu Liu, Azadeh Alavi, Minyi Li, and Xiang Zhang. Self-supervised contrastive learning for medical time series: A systematic review. *Sensors*, 23(9):4221, 2023.

Appendix A Dataset Details

We use five diverse time series datasets to evaluate our model. Following is a detailed description of the datasets.

DEAP dataset [18]. The publicly available database DEAP consists of a multimodal dataset for the analysis of human emotional states. A total of 32 EEG channels and eight peripheral physiological signals of 32 subjects (aged between 19 and 37) were recorded whilst watching music videos with a sampling frequency of 128 Hz. Then the recorded signals are passed from a bandpass filter to remove noise and artifacts like eye blinks. The 40 one-minute-long videos were carefully selected to elicit different emotional states according to the dimensional, valence-arousal. The valence-arousal emotion model, first proposed by Russell [1], places each emotional state on a two-dimensional scale. The first dimension represents valence, which ranged from negative to positive, and the second dimension is arousal, which ranged from calm to exciting. In DEAP, each video clip is rated from 1 to 9 for arousal and valence by each subject after the viewing, and the discrete rating value can be used as a classification label in emotion recognition [2–6].

SEED dataset [44]. The SJTU Emotion EEG Dataset (SEED) is a free and publicly available EEG dataset for emotional analysis provided by Shanghai Jiao Tong University in 2015. SEED dataset provided EEG recordings from 15 subjects (8 females and 7 males, 23.27 ± 2.37 years) using a 62-channel system. In total, 45 trials (the same 15 movie clips repeated on 3 days) were presented to the subjects. Each trial lasted for approximately 4 minutes. Each participant contributed to the experiment thrice at an interval of one week or longer. For data preprocessing, these recordings were downsampled from 1000 to 200 Hz and filtered to 0.5–70 Hz. In addition, the labels of the trials were obtained from the self-assessments, and the elicitations involved three emotional categories: positive, neutral, and negative.

P19 dataset [47]. P19 (PhysioNet Sepsis Early Prediction Challenge 2019) dataset contains 38,803 patients and each patient is monitored by 34 irregularly sampled sensors including 8 vital signs and 26 laboratory values. The original dataset has 40,336 patients, we remove the samples with too short or too long time series, remaining 38,803 patients (the longest time series of the patient has more than one and less than 60 observations). Each patient is associated with a static vector indicating attributes: age, gender, time between hospital admission and ICU admission, ICU type, and ICU length of stay (days). Each patient has a binary label representing occurrence of sepsis within the next 6 hours. The dataset is highly imbalanced with only ~4% positive samples. Raw data of P19 can be found at <https://physionet.org/content/challenge-2019/1.0.0/>.

EPILEPSY dataset [45]. The dataset contains single-channel EEG measurements from 500 subjects. For every subject, the brain activity was recorded for 23.6 seconds. The dataset was then divided and shuffled (to mitigate sample-subject association) into 11,500 samples of 1 second each, sampled at 178 Hz. The raw dataset features five classification labels corresponding to different states of subjects or measurement locations — eyes open, eyes closed, EEG measured in the healthy brain region, EEG measured in the tumor region, and whether the subject has a seizure episode. To emphasize the distinction between positive and negative samples in terms of epilepsy, We merge the first four classes into one, and each time series sample has a binary label describing if the associated subject is experiencing a seizure or not. There are 11,500 EEG samples in total. The raw dataset (<https://repositori.upf.edu/handle/10230/42894>) is distributed under the Creative Commons License (CC-BY) 4.0.

HAR [46]. This dataset contains recordings of 30 health volunteers performing daily activities, including walking, walking upstairs, walking downstairs, sitting, standing, and lying. Prediction labels are the six activities. The wearable sensors on a smartphone measure triaxial linear acceleration and triaxial angular velocity at 50 Hz. After preprocessing and isolating gravitational acceleration from body acceleration, there are nine channels (i.e., 3-axis accelerometer, 3-axis gyroscope, and 3-axis magnetometer) in total. The raw dataset (<https://archive.ics.uci.edu/ml/datasets/Human+Activity+Recognition+Using+Smartphones>) is distributed as-is. Any commercial use is not allowed.

Appendix B Experimental Details

We implement the baselines follow the corresponding papers including TS2vec [26], Mixing-up [28], TS-TCC [27], SimCLR [11], and TFC [29]. Unless noted below, we use default settings for hyper-parameters as reported in the original works. All two-stage and end-to-end frameworks with baselines are done with an NVIDIA GeForce RTX 3090 GPU with 256 GB of allocated memory.

SLOTS (our model) allows for the simultaneous training of the encoder and classifier, unifying model optimization, reducing intermediate computational resources, and learning task-specific features. Our encoder f is similar to ECNN-C [15]. Specifically, the novel block structure is designed to comprise four different convolutional layers. First, we adopt two consecutive kernels 3×1 and 1×3 to replace the convolution kernel of shape of 3×3 by taking a similar operation to MobileNet model. Second, we use spatial convolution with a depth multiplier of 2, thus doubling the number of channels in the first deep convolution layer. The purpose of this approach is to enable the model to have sufficient channels, allowing them to utilize a reduction factor in bottleneck structures [49]. Third, separable pooling is used to replace the max-pooling due to the aliasing in the step convolution. We adopt a 2×1 pooling kernel after the first spatial convolutional layer. The classifier contains one fully-connected layer. We employ a specific data augmentation technique for the proposed algorithm. This involves masking the data using a binary mask, where each element is independently sampled from a Bernoulli distribution with a probability of $p=0.5$. We use a batch size of 100 and a training epoch of 30.

TS2Vec [26] introduces the notion of contextual consistency and uses a hierarchical loss function to capture long-range structure in time series. TS2vec is a powerful representative learning method and has a specially-designed architecture. The encoder network consists of three components. First, the input time series is augmented by selecting overlapping subseries. They are projected into a higher dimensional latent space. Then, latent vectors for input time series are masked at randomly chosen positions. Finally, a dilated CNN with residual blocks produces the contextual representations. To compute the loss, the representations are gradually pooled along the time dimension and at each step a loss function based on contextual consistency is applied. For the baseline experiment, we found that the original 10 layers of ResNet blocks are redundant, and we reduce residual blocks in the encoder from 10-layer to 3-layer without compromising model performances.

Mixing-up [28] proposes new mixing-up augmentation and pretext tasks that aim to correctly predict the mixing proportion of two time series samples. In Mixing-up, the augmentation is chosen as the convex combination of two randomly drawn time series from the dataset, where the mixing parameter is random drawn from a beta distribution. The contrastive loss is then computed between the two inputs and the augmented time series. The loss is a minor modification of NT-Xent loss and is designed to encourage the correct prediction of the amount of mixing. We use the same beta distribution as reported in the original Mixing-up model.

TS-TCC [27] leverages contextual information with a transformer-based autoregressive model and ensures transferability by using both strong and weak augmentations. TS-TCC proposed a challenging pretext task. An input time series sample is first augmented by adding noise, scaling, and permuting time series. The views are then passed through an encoder consisting of three convolutional layers before being processed by the temporal contrasting module. During temporal contrasting, for each view, a transformer architecture is used to learn a contextual representation. The learned representation is then used to predict latent observation of the other augmented view at a future time. The contextual representations are then projected and maximized similarity using NT-Xent loss. For this baseline, we mostly adopted the hyper-parameters presented in the original paper.

SimCLR [11] is a state-of-the-art model in self-supervised representation learning of images. It utilizes deep learning architectures to generate augmentation-based embeddings and optimize the model parameters by minimizing NT-Xent loss in the embedding space. Although initially proposed for image data, it is readily adapted to time series, as shown in [27]. An input time series sample is first augmented into two related views. Then a base encoder extracts representation vectors. ResNet is used as an encoder backbone for simplicity. Then the projection head transforms representations into a latent space where the NT-Xent loss is applied. For time series, SimCLR investigated two augmentations, including jitter-and-scale, and permutation-and-jitter. All the unmentioned hyper-parameters are kept the same as the original model.

TFC [29] introduces a strategy for self-supervised pre-training in time series by modeling Time-Frequency Consistency. TFC specifies that time-based and frequency-based representations, learned from the same time series sample, should be closer to each other in the time-frequency space than representations of different time series samples. Specifically, contrastive learning in time-space is adapted to generate a time-based representation. In parallel, TFC proposes a set of novel augmentations based on the characteristic of the frequency spectrum and produces a frequency-based embedding through contrastive instance discrimination. All the unmentioned hyper-parameters are kept the same as the original model.

Appendix C Extended Experimental Results

Table 5 is the performance with errorbars comparison on SEED, P19, EPILEPSY, and HAR, under the label ratio of 10%.

Appendix D Additional Information on Robustness Validation

We investigate the robustness of SLOTS in three settings on DEAP dataset: trial-dependent, leave-trials-out, and leave-subjects-out [7–10]. The details of these three settings are explained as follows.

1) Trial-dependent

In the DEAP dataset, we permute the trials of 32 subjects and randomly selected some trials as the training set and the remaining trials as the testing set.

2) Leave-trials-out

In the DEAP dataset, each subject has 40 trials. We take out some of their trials for each of the 32 subjects to form the training set, and the remaining trials to form the testing set. For example, the first 36 trials are used as the training set and the last 4 trials as the testing set. The total number of trials in the training set is $36 \times 32 = 1152$; the total number of trials in the testing set is $4 \times 32 = 128$.

3) Leave-subjects-out

In the DEAP dataset, there are a total of 32 subjects. We randomly select a part of the subjects as the training set and a part of the subjects as the testing set. For example, 30 subjects are randomly selected as the training set and the remaining 2 subjects as the testing set. The total number of trials in the training set is $30 \times 40 = 1200$; the number of trials in the test set is $2 \times 40 = 80$.

Appendix E Transferability of SLOTS

We note the trade-off between adaptability and model performance. While two-stage models may be more effective in transfer learning or situations where pre-training and fine-tuning involve different datasets, our SLOTS model is a superior choice for achieving optimal performance on a specific dataset (Section 5).

In the two-stage framework, we use the DEAP dataset during pre-training and the SEED dataset during fine-tuning. We report metrics including accuracy, precision (macro-averaged), recall, F1-score, AUROC (one-versus-rest), and AUPRC. The evaluation results are shown in Table 6.

Table 5: Performance with errorbars comparison on SEED, P19, EPILEPSY, and HAR, under the label ratio of 10%.

Models	SEED					
	Accuracy	Precision	Recall	F1 score	AUROC	AUPRC
TS2Vec	0.5750 \pm 0.0561	0.6048 \pm 0.0751	0.5732 \pm 0.0836	0.5113 \pm 0.1023	0.6493 \pm 0.0651	0.6218 \pm 0.0712
TS2Vec++	0.6252 \pm 0.0695	0.6191 \pm 0.0752	0.6084 \pm 0.0658	0.5599 \pm 0.0832	0.6607 \pm 0.0694	0.6962 \pm 0.0769
TS-TCC	0.5893 \pm 0.0852	0.5627 \pm 0.0935	0.5772 \pm 0.0876	0.5723 \pm 0.0987	0.7137 \pm 0.0876	0.6941 \pm 0.0635
TS-TCC++	0.6172 \pm 0.0845	0.5935 \pm 0.0657	0.5776 \pm 0.0589	0.5977 \pm 0.0896	0.8004 \pm 0.0674	0.7637 \pm 0.0863
SimCLR	0.5050 \pm 0.0651	0.5115 \pm 0.0769	0.5313 \pm 0.0984	0.5155 \pm 0.0863	0.6963 \pm 0.0785	0.6982 \pm 0.0895
SimCLR++	0.5736 \pm 0.0782	0.5344 \pm 0.0972	0.5505 \pm 0.0871	0.5374 \pm 0.0777	0.6802 \pm 0.0698	0.6361 \pm 0.0974
MixUp	0.5166 \pm 0.0642	0.5356 \pm 0.0759	0.5638 \pm 0.0968	0.5141 \pm 0.0874	0.6605 \pm 0.0778	0.6580 \pm 0.0965
MixUp++	0.5569 \pm 0.0869	0.5701 \pm 0.0759	0.5638 \pm 0.0963	0.5265 \pm 0.0758	0.7494 \pm 0.0851	0.6603 \pm 0.0685
TFC	0.5500 \pm 0.0542	0.5356 \pm 0.0693	0.5487 \pm 0.0579	0.5290 \pm 0.0698	0.7499 \pm 0.0782	0.6423 \pm 0.0869
TFC++	0.6087 \pm 0.0368	0.6071 \pm 0.0597	0.6071 \pm 0.0698	0.5990 \pm 0.0475	0.7847 \pm 0.0369	0.6685 \pm 0.0475
SLOTS(two-stage)	0.6468 \pm 0.0682	0.6573 \pm 0.0864	0.7316 \pm 0.0987	0.6169 \pm 0.0996	0.7575 \pm 0.0874	0.7572 \pm 0.0872
SLOTS(end-to-end)	0.7181 \pm 0.1023	0.7286 \pm 0.0964	0.7869 \pm 0.0867	0.6510 \pm 0.1136	0.8034 \pm 0.0987	0.7592 \pm 0.0869

Models	P19					
	Accuracy	Precision	Recall	F1 score	AUROC	AUPRC
TS2Vec	0.6580 \pm 0.0562	0.6467 \pm 0.0634	0.5520 \pm 0.0675	0.5669 \pm 0.0741	0.5171 \pm 0.0683	0.5860 \pm 0.0652
TS2Vec++	0.6589 \pm 0.0358	0.6794 \pm 0.0210	0.6500 \pm 0.0235	0.6894 \pm 0.0355	0.6527 \pm 0.0196	0.6978 \pm 0.0210
TS-TCC	0.9216 \pm 0.0325	0.5968 \pm 0.0413	0.6597 \pm 0.0321	0.6156 \pm 0.0369	0.6941 \pm 0.0299	0.6667 \pm 0.0345
TS-TCC++	0.9654 \pm 0.0681	0.7338 \pm 0.0593	0.6776 \pm 0.0581	0.7076 \pm 0.0698	0.7011 \pm 0.0782	0.7065 \pm 0.0635
SimCLR	0.9130 \pm 0.0594	0.5877 \pm 0.0425	0.5600 \pm 0.0501	0.5338 \pm 0.0632	0.5995 \pm 0.0596	0.5956 \pm 0.0720
SimCLR++	0.9534 \pm 0.0368	0.6924 \pm 0.0244	0.6124 \pm 0.0543	0.6321 \pm 0.0576	0.7077 \pm 0.0147	0.6554 \pm 0.0247
MixUp	0.9136 \pm 0.0369	0.6744 \pm 0.0475	0.6481 \pm 0.0355	0.6477 \pm 0.0593	0.6802 \pm 0.0682	0.6361 \pm 0.0651
MixUp++	0.9253 \pm 0.0741	0.6777 \pm 0.0655	0.6500 \pm 0.0357	0.6489 \pm 0.0698	0.7685 \pm 0.0241	0.6932 \pm 0.0369
TFC	0.9049 \pm 0.0357	0.6207 \pm 0.0366	0.6340 \pm 0.0445	0.6267 \pm 0.0369	0.6399 \pm 0.0485	0.7092 \pm 0.0436
TFC++	0.9361 \pm 0.0563	0.7500 \pm 0.0684	0.6761 \pm 0.0536	0.6954 \pm 0.0458	0.7721 \pm 0.0412	0.7287 \pm 0.0369
SLOTS(two-stage)	0.9254 \pm 0.0842	0.7138 \pm 0.0933	0.6776 \pm 0.0789	0.7076 \pm 0.1023	0.7011 \pm 0.0698	0.7065 \pm 0.0563
SLOTS(end-to-end)	0.9596 \pm 0.1036	0.7580 \pm 0.1025	0.7416 \pm 0.1124	0.7788 \pm 0.1253	0.7703 \pm 0.0865	0.8270 \pm 0.0869

Models	EPILEPSY					
	Accuracy	Precision	Recall	F1 score	AUROC	AUPRC
TS2Vec	0.5125 \pm 0.0569	0.5604 \pm 0.0647	0.5118 \pm 0.0541	0.5287 \pm 0.0698	0.6519 \pm 0.0754	0.6233 \pm 0.0694
TS2Vec++	0.6022 \pm 0.0658	0.6011 \pm 0.0794	0.5500 \pm 0.0635	0.5445 \pm 0.0774	0.6537 \pm 0.0896	0.6498 \pm 0.0894
TS-TCC	0.6175 \pm 0.0313	0.6338 \pm 0.0779	0.5000 \pm 0.0312	0.5403 \pm 0.0510	0.6029 \pm 0.0122	0.6726 \pm 0.0097
TS-TCC++	0.6206 \pm 0.0818	0.6401 \pm 0.0938	0.5459 \pm 0.0936	0.5445 \pm 0.0928	0.6851 \pm 0.0678	0.7150 \pm 0.0715
SimCLR	0.6375 \pm 0.0751	0.5938 \pm 0.0698	0.5200 \pm 0.0876	0.5100 \pm 0.0964	0.6293 \pm 0.0854	0.6776 \pm 0.0769
SimCLR++	0.6805 \pm 0.0984	0.6591 \pm 0.0842	0.5084 \pm 0.0687	0.5599 \pm 0.0964	0.6607 \pm 0.0578	0.6962 \pm 0.0635
MixUp	0.6175 \pm 0.0778	0.6115 \pm 0.0863	0.5313 \pm 0.0684	0.5485 \pm 0.0851	0.6596 \pm 0.0657	0.6782 \pm 0.0423
MixUp++	0.6617 \pm 0.0412	0.6356 \pm 0.0324	0.5804 \pm 0.0256	0.5734 \pm 0.0421	0.6605 \pm 0.0332	0.6980 \pm 0.0236
TFC	0.6550 \pm 0.0369	0.6312 \pm 0.0475	0.5250 \pm 0.0452	0.5226 \pm 0.0637	0.5390 \pm 0.0635	0.6653 \pm 0.0569
TFC++	0.6693 \pm 0.0786	0.6627 \pm 0.0684	0.5472 \pm 0.0756	0.5472 \pm 0.0692	0.7014 \pm 0.0462	0.6834 \pm 0.0553
SLOTS(two-stage)	0.6652 \pm 0.0896	0.6591 \pm 0.0974	0.5684 \pm 0.0963	0.5599 \pm 0.0823	0.6607 \pm 0.0785	0.6962 \pm 0.0862
SLOTS(end-to-end)	0.6955 \pm 0.1102	0.6952 \pm 0.0962	0.5999 \pm 0.1084	0.5819 \pm 0.1024	0.7105 \pm 0.0984	0.7600 \pm 0.0893

Models	HAR					
	Accuracy	Precision	Recall	F1 score	AUROC	AUPRC
TS2Vec	0.5738 \pm 0.0125	0.5555 \pm 0.0241	0.5768 \pm 0.0362	0.5565 \pm 0.0452	0.7623 \pm 0.0123	0.7413 \pm 0.0163
TS2Vec++	0.6743 \pm 0.0698	0.6197 \pm 0.0541	0.5838 \pm 0.0751	0.5701 \pm 0.0832	0.8488 \pm 0.0564	0.8114 \pm 0.0452
TS-TCC	0.6596 \pm 0.0079	0.6154 \pm 0.0115	0.6158 \pm 0.0266	0.5459 \pm 0.0120	0.7511 \pm 0.0077	0.7414 \pm 0.0112
TS-TCC++	0.6787 \pm 0.0128	0.6473 \pm 0.0093	0.6316 \pm 0.0096	0.6169 \pm 0.0005	0.7575 \pm 0.0053	0.7572 \pm 0.0159
SimCLR	0.6168 \pm 0.0347	0.6390 \pm 0.0478	0.5704 \pm 0.0563	0.5744 \pm 0.0698	0.7452 \pm 0.0452	0.7098 \pm 0.0365
SimCLR++	0.6217 \pm 0.0657	0.6435 \pm 0.0593	0.6205 \pm 0.0741	0.5977 \pm 0.0863	0.9004 \pm 0.0634	0.7637 \pm 0.0413
MixUp	0.6277 \pm 0.0421	0.6393 \pm 0.0325	0.6138 \pm 0.0415	0.6055 \pm 0.0365	0.7705 \pm 0.0214	0.7481 \pm 0.0259
MixUp++	0.6699 \pm 0.0358	0.6577 \pm 0.0563	0.6541 \pm 0.0684	0.6172 \pm 0.0687	0.8878 \pm 0.0632	0.8254 \pm 0.0412
TFC	0.6502 \pm 0.0658	0.6102 \pm 0.0753	0.6083 \pm 0.0861	0.6095 \pm 0.0742	0.7315 \pm 0.0436	0.7371 \pm 0.0438
TFC++	0.7263 \pm 0.0362	0.6479 \pm 0.0214	0.6634 \pm 0.0421	0.6512 \pm 0.0369	0.8519 \pm 0.0128	0.8064 \pm 0.0231
SLOTS(two-stage)	0.6654 \pm 0.0896	0.6538 \pm 0.0968	0.6276 \pm 0.0785	0.6076 \pm 0.0993	0.8011 \pm 0.0741	0.7565 \pm 0.0635
SLOTS(end-to-end)	0.7312 \pm 0.0936	0.6661 \pm 0.0967	0.6720 \pm 0.0786	0.6615 \pm 0.1036	0.9013 \pm 0.0997	0.8811 \pm 0.0974

Table 6: Performance of baseline and SLOTS: pre-training on DEAP and fine-tuning on SEED.

Models	Accuracy	Precision	Recall	F1 Score	AUROC	AUPRC
TS2Vec	0.5781 \pm 0.0281	0.5683 \pm 0.0272	0.5325 \pm 0.0351	0.5278 \pm 0.0315	0.7488 \pm 0.0193	0.6151 \pm 0.0252
TS-TCC	0.4937 \pm 0.0250	0.5516 \pm 0.0147	0.4870 \pm 0.0275	0.4859 \pm 0.0202	0.6915 \pm 0.0332	0.5674 \pm 0.0101
SimCLR	0.5312 \pm 0.0312	0.5472 \pm 0.0363	0.5248 \pm 0.0284	0.5154 \pm 0.0252	0.7363 \pm 0.0173	0.6206 \pm 0.0159
MixUp	0.4875 \pm 0.0437	0.4832 \pm 0.0377	0.4878 \pm 0.0275	0.4647 \pm 0.0390	0.6887 \pm 0.0382	0.5677 \pm 0.0332
TFC	0.6031 \pm 0.0093	0.6135 \pm 0.0315	0.6028 \pm 0.0239	0.5847 \pm 0.0272	0.7900 \pm 0.0020	0.6642 \pm 0.0206
SLOTS (two-stage)	0.5250 \pm 0.0062	0.5313 \pm 0.0185	0.5215 \pm 0.0112	0.5180 \pm 0.0122	0.7176 \pm 0.0050	0.5928 \pm 0.0014

Appendix References

- [S1] James A Russell. A circumplex model of affect. *Journal of Personality and Social Psychology*, 39(6):1161–1178, 1980.
- [S2] Arvid Frydenlund and Frank Rudzicz. Emotional affect estimation using video and EEG data in deep neural networks. In *Canadian Conference on Artificial Intelligence*, pages 273–280, 2015.
- [S3] Tien Pham, Wanli Ma, Dat Tran, Duc Su Tran, and Dinh Phung. A study on the stability of EEG signals for user authentication. In *International IEEE/EMBS Conference on Neural Engineering*, pages 122–125, 2015.
- [S4] Zirui Lan, Olga Sourina, Lipo Wang, and Yisi Liu. Real-time EEG-based emotion monitoring using stable features. *The Visual Computer*, 32:347–358, 2016.
- [S5] Hao Chao and Liang Dong. Emotion recognition using three-dimensional feature and convolutional neural network from multichannel EEG signals. *IEEE Sensors Journal*, 21(2):2024–2034, 2021.
- [S6] Sara Bagherzadeh, Keivan Maghooli, Ahmad Shalbaf, and Arash Maghsoudi. Emotion recognition using effective connectivity and pre-trained convolutional neural networks in EEG signals. *Cognitive Neurodynamics*, 16:1087–1106, 2022.
- [S7] Zhen Liang, Rushuang Zhou, Li Zhang, Linling Li, Gan Huang, Zhiguo Zhang, and Shin Ishii. EEGFuseNet: Hybrid unsupervised deep feature characterization and fusion for high-dimensional EEG with an application to emotion recognition. *IEEE Transactions on Neural Systems and Rehabilitation Engineering*, 29:1913–1925, 2021.
- [S8] Nandini Kumari, Shamama Anwar, and Vandana Bhattacharjee. Time series-dependent feature of EEG signals for improved visually evoked emotion classification using emotioncapsnet. *Neural Computing and Applications*, 34:13291–13303, 2022.
- [S9] Byung Hyung Kim and Sungho Jo. Deep physiological affect network for the recognition of human emotions. *IEEE Transactions on Affective Computing*, 11(2):230–243, 2020.
- [S10] Ahmet Mert and Aydin Akan. Emotion recognition from EEG signals by using multivariate empirical mode decomposition. *Pattern Analysis and Applications*, 21:81–89, 2018.